Jurnal Kejuruteraan 38(7) 2026: 3471-3481
https://doi.org/10.17576/jkukm-2026-38(7)-25

Enhancing Experimental Reliability Through Rainfall Simulator Calibration Under Intense Rainfall Rates

Mohamad Syazwan Mohd Roslee[a], Vynotdni Rathinasamy[a*], Ahmad Zharfan Ahmad Husaini[a], Mastura Azmi[a], Anis Adriana Mohd Rashid[a], Mohd Firdaus Md Dan[c] & Dayang Zulaika Abang Hasbollah[b]

[a]*School of Civil Engineering, Universiti Sains Malaysia, 14300 Nibong Tebal, Pulau Pinang, Malaysia.*

[b]*Geotropik Centre, Faculty of Civil Engineering, Universiti Teknologi Malaysia, 81310 Skudai, Johor Bahru, Malaysia.*

[c]*Faculty of Civil and Environmental Engineering, Universiti Tun Hussein Onn Malaysia, 86400 Parit Raja, Johor, Malaysia.*

[*]*Corresponding author: vynotdni@usm.my*

Received 5 November 2025, Received in revised form 23 June 2026
Accepted 23 July 2026, Available online 30 October 2026

ABSTRACT

Acknowledging the benefit of Rainfall Simulators (RS) is continuously growing among researcher, mainly for laboratory-scale models where natural rainfall is either unavailable or inconsistent. RS put forward a reliable platform for replicating specific rainfall events under standardized set-up, making them invaluable for erosion, hydrology, and slope stability research needs. The present work offered a cost-effective Dripping Rainfall Simulator (DRS) for application on a 1.2 m² test plot area. After several standardizations, the DRS that produces replicable storms of rainfall (at 60 mm/hr and 120 mm/hr) demonstrated satisfactory spatial uniformity, with Christiansen's uniformity coefficients (CUC) coverage ranging from 81.18–88.69% distribution across the monitoring plot. Additionally, the mean diameters (D_m) and median volumetric drop diameters (D_{50}), measured using a flour-pellet method, were found to extend from 3.8–4.4 mm and 2.7–3.1 mm independently which line up well with values reported in previous research. The relative terminal velocity (V_r) calculated was attained to range between 8.59–8.92 m/s with energy flux from 36.88 to 39.77 J/mm/m². These findings verify the RS capability to replicate natural rainfall with considerable accuracy let alone provide a strong foundation to be used in future applications in experimental modelling. From the basis of this study regarding RS, researchers will be able to create events-scale physical models in their relevant engineering areas.

Keywords: Rainfall simulator; rainfall rates; spatial uniformity; terminal velocity (V_T); kinetic energy (KE)

INTRODUCTION

Rainfall Simulators (RS) have become a major aspect of laboratory research because of their wide-ranging applications in multiple fields. These devices are helping researchers by replicating precipitations in a controlled environment, which enables the systematic study of soil behavior and structural responses (Ren et al. 2022; Li et al. 2025; Nguyen et al. 2025) without the need to wait for storms that are unpredictable. They are also fundamental for studying water infiltration (Ren et al. 2021), runoff generation (Pietro et al. 2021), sediment transport (Kinnell 2022) as well as being relied for calibrating hydrological models to understand the impact of climate change on land degradation (Anderson et al. 2021).

However, to fully harness their potential, it is critical that RS accurately provides the key features of rainfall especially with high intensities. Intense rainfall influences various geotechnical and hydrological processes, making it an important factor to consider in related experimental studies (Rajamoorthy & Munusamy 2018; Idrus et al. 2023; Ehsan et al. 2024; Hamizak et al. 2024). Rainfall with higher kinetic energy (*KE*) tends to exert stronger erosive forces on the soil surface (Yang et al. 2025). In-depth investigations have shown that intense rainfall contributes to greater soil displacement by delivering substantial energy upon impact (Suif et al. 2025).

Despite advancements, RS faces ongoing issues such as oversized drops, mismatched droplet terminal velocities (V_T) and inaccurate droplet distribution (Bosio et al. 2023;

Lazarus et al. 2023) when compared to natural rainfall criteria. This phenomenon happens when water or droplets are released under gravitational force, they begin from rest and accelerate (D'Angelo et al. 2022) until they reach a V_T, which varies based on their diameter. Smaller droplets, having lower mass, attain this terminal speed more quickly and require less height to do so (Gabyshev et al. 2022).

The uniformity coefficient (CU) is commonly used to represent the evenness of rainfall distribution within a test area as a single percentage (Živanović et al. 2022; Li et al. 2023; Kalehhouei et al. 2025). This application to larger or more complex surfaces has drawn criticism for overlooking localized variability. For example, an assessment by Green and Pattison (2022) raises an issue that although many sampling points may report rainfall depths close to the average, its reliance on a single numerical value fails to reflect small-scale differences, often leading to a misleading impression of uniformity. The overemphasis on achieving "perfect" uniformity seems counterproductive as it ignores the natural variability of rainfall and may misguide research priorities. To address these issues, the authors recommend using CU in repeat testing to enhance the spatial and temporal variability of rainfall simulation assessments. Despite its limitations, it remains widely used due to its simplicity and historical significance, with only minor adjustments proposed in recent studies for more refined evaluation metrics (Green & Pattison 2022).

RS can also be distinguished by their operational systems being either gravity-fed or pressure-driven type. Gravity-fed RS type relies on natural drip mechanisms to create rainfall by its dripping principles. These are simple and energy-independent way but the key limitation of this type is it tends to produce oversized droplets (Lanza et al. 2021) and the shorter fall heights (normally less than 10 m) often prevent drops from reaching adequate *KE* and V_T (Fernández et al. 2022). Additionally, the droplet sizes tend to be uniform across the test area (Fernández et al. 2022).

In contrast, pressure-driven RS pump water from a ground reservoir to elevated nozzles, creating finer droplets. While these systems are lighter and easier to transport, the atomized water droplets often travel at speeds higher than those observed in natural rainfall, due to the pressure applied by the pump. Using identical nozzles produces uniform drop sizes, though combining different nozzle types can typically simulate more realistic raindrop distributions (Yonter & Houndonougbo 2022). By adjusting nozzle height, different rainfall intensities and energy levels can also be achieved (Costa et al. 2024). Both types have certain limitations as discussed. In short, the gravity-based systems struggle to achieve natural droplet speeds while the pressure-driven systems often produce non-natural droplet mass.

RS can be categorized based on test site whether they are being used as portable models for field studies or fixed systems typically installed in laboratories. Fixed setups generally offer greater control over variables like water quality and drops height, but they face constraints such as limited space. Meanwhile, portable designs are in favor of lightness and mobility for use in remote or challenging terrains.

As summarized in Table 1, which provides and compares a comparative overview of the key characteristics of various RS designs reported in recent literature, it is observed that most of the raindrops created by current RS used in field studies often tend to be significantly larger than what naturally falls.

To address such discrepancy, this paper presents a newly developed RS specifically engineered to better replicate the *KE*, V_T and droplet characteristics of natural rainfall.

TABLE 1. Comparative summary of design features and performance of RS systems as reported in literature.

Simulator type	Drop forming apparatus	Rainfall intensity (mm/hr)	Christiansen uniformity	Drop size (mm)	Simulation area (m^2)	Rainfall continuum	Height (m)	Portability	Researcher
Spraying nozzle	Two nozzles with solenoid valves	4–82	0.73 at 82 mm/hr	-	2.78	Continuous	2.4–3	Not portable	(Renner et al. 2024)
Spraying nozzle	Five square pattern nozzles	100	0.87	0.75-7	1, 1.96	Continuous	1.9	Portable	(Tiller et al. 2025)
Spraying nozzle	Five pressurized nozzles	21–79	0.8-0.93	0.38–2.11	4.5	Continuous	12	Not portable	(Jadhao et al. 2023a)
Dripper & nebulizer	Random arrangement nozzles	-	0.25–0.94	-	0.0025 sample range	Continuous	10	Not portable	(Fernández et al. 2022)
Dripper	1 m laterals each with 10 drippers.	40–80	0.96-0.98	3.0–3.4	0.793	Continuous	1.5	Not portable	(Ramli et al. 2021)

METHODOLOGY

MATERIALS AND SETUPS

For this project, the location of the DRS was an exterior yard at the School of Civil Engineering, Universiti Sains Malaysia. Available space and structural constraints necessitated the use of a 2 m height in this study. Despite these constraints, the DRS was calibrated to ensure realistic uniformity, consistent with criteria reviewed by Rončević et al. (2022). Our model mirrors their documented optimization of feed-line configuration to stabilize water pressure in which the 2 m height corresponds to the most adopted standard, where heights up to 2 m are most used to balance structural support limitations (Rončević et al. 2022). While this 2 m drop height does not ensure the raindrops to reach their true natural terminal velocity which typically requires a fall distance of 7 to 9 meters, it provides a standardized environment for testing. Consequently, the setup remains fully valid for future erosion interpretations when making relative comparisons as a benchmark. The development of the DRS was improved in several stages as improvements were made.

DESIGN OF THE DRIPPING RAINFALL SIMULATOR (DRS)

The DRS developed in this study was designed for use over a 1.2 m^2 rainfall catchment area (RCA) measuring 1.0 m × 1.2 m, aligning with best practices that recommend a minimum experimental plot size of 1 m^2 (Boulange et al. 2019). It was specifically configured to cover two separate sections, corresponding to the two-part model tank with an overall dimension of 1.2 m × 1.0 m × 1.0 m. Water is conveyed from the water tank through a hose pipe via a submersible pump (HCP Pond Series Submersible Sump Pump) which connects to a Y-shaped fitting. From there, the flow is split into two of 4-outlets distributor that directs the water to individual feeding tubes. These feeding tubes then channel the water to the drippers. The feeding tube is made of Polyethylene with an internal diameter of 4 mm. To maintain precise control over the hydraulic conditions, adjustable valves and a flow meter are integrated into the system, enabling fine-tuning of nozzle pressure and ensuring a stable discharge rate of 72 and 144 L/hr throughout the experimental procedures as illustrated in Figure 1.

FRAMING SYSTEM

The structural frame of the DRS is made of Dexion steel. Its main function is to provide structural support for connecting with the feeding tubes and drippers. As illustrated in Figure 2(a) and 2(b), the system comprises twelve laterals. Each 1 m long lateral housed ten uniformly spaced emitters with horizontal and vertical intervals at 0.9 m and 0.86 m respectively. The DRS was systematically divided into two distinct sections RS1 for the six upper part and RS2 for the other lower part. A pre-existing steel-framed shelter at the site served as the foundation for mounting the DRS structural frame model. The model was firmly secured to the structure by bolting its edges directly onto the steel frame.

DRIP-TYPE RAINFALL EMITTER UNIT

The rainfall simulation system utilized 120 units of Polypropylene Rainjet adjustable drippers, specifically model 91217 by the *Claber* brand each capable of delivering up to 6 L/hr. Each dripper estimated to produce a spray diameter of approximately 4 mm.

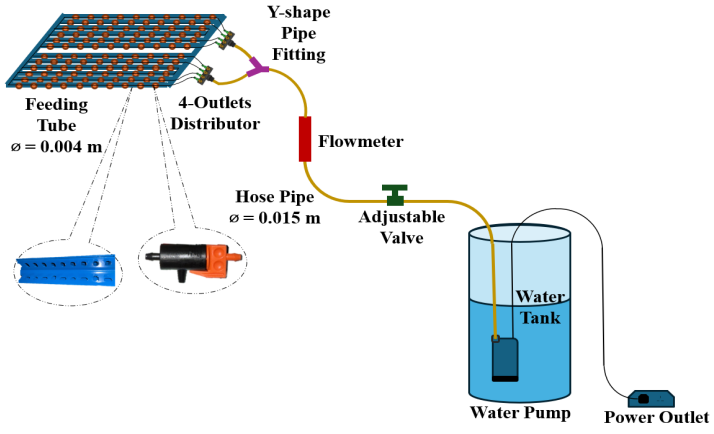


FIGURE 1. Overall schematic diagram of the water distribution system

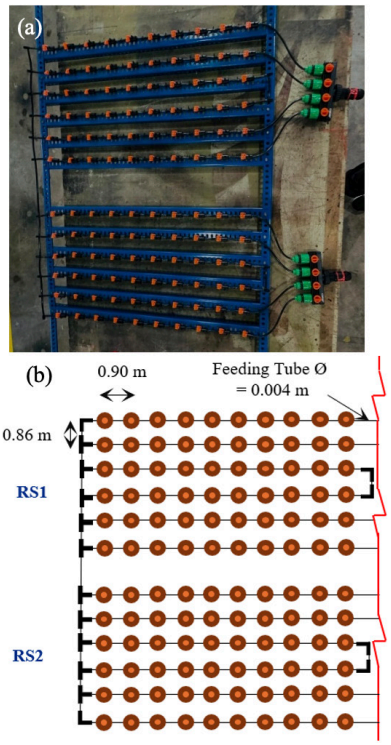


FIGURE 2. Fabricated rainfall model (a) on site-image and (b) schematic diagram

CALIBRATION OF RAINFALL INTENSITY

In this study, targeted rainfall intensities of 60 and 120 mm/hr were established by regulating pump pressure via the adjustable valve system. The intensities reflect representative heavy rainfall scenarios (Zhang et al. 2020; Xiao et al. 2024) commonly observed in tropical climates. The actual rainfall delivered over the RCA was empirically verified by collecting the surface runoff within an hour in a 1.2 m^2 collection tank (1 m × 1.2 m × 1 m) which was divided into two equal sections.

CALIBRATION OF RAINFALL SPATIAL UNIFORMITY

Natural rainfall is inherently influenced by dynamic atmospheric and geographical conditions, resulting in considerable variability (Felipe et al. 2024). In contrast, a good RS must deliver rainfall in a controlled, consistent, and repeatable manner (Lazarus et al. 2023) to ensure experimental accuracy and reproducibility. Calibration is thus essential to address potential discrepancies caused by emitter inconsistencies, wind interference, and internal system pressure variations (Maroufpoor et al. 2010). The Christiansen uniformity coefficients (CUC), developed by J.E. Christiansen (1942), was initially used to evaluate the uniformity of irrigation systems and has since become a standard metric for assessing rainfall distribution in simulation studies (Bosio et al. 2023; Costa et al. 2023). Additional models, such as those proposed by Hart and Reynolds and specialists from the Hawaiian Cane Society, have also been used in similar contexts which produced percentage of uniformity coefficients comparable to those of the CUC (45% to 80%) (Maroufpoor et al. 2010).

To obtain quantitative data, rainfall was collected using fifteen cups with 70 mm in diameter and 20 mL capacity (Jadhao et al. 2023b), which were randomly positioned on a circular wooden platform approximately 0.6 m in diameter. This platform was positioned directly beneath each section of the RS in turn. Rainfall was allowed to accumulate in the cups within the target area over a standardized duration of five minutes, after which the collected volumes were measured. The spatial uniformity of the simulated rainfall distribution was then evaluated using the CUC, calculated using the formula as follows:

$$\mathrm{CUC} = 100\,[1 - (\Sigma|x - \bar{x}| / (n\bar{x}))] \quad (1)$$

where CUC represents the spatial uniformity of the applied rainfall, x denotes the amount of water in an individual cup (mL) and $\bar{x}$ is the mean average amount of water in all n cups (mL). The resulting CUC value was interpreted based on the following classification scale: values above 90% indicate Excellent uniformity, 80–90% is considered Good, 70–80% is Fair, 60–70% is Poor, and values below 60% are deemed Unacceptable.

CALIBRATION OF RAINFALL DROPLET SIZE DISTRIBUTION

The distribution size of raindrops can be used to classify the type of precipitation (Jwa et al. 2021) and different experimental methods for estimating drop size have been developed to estimate drop size from simulated or natural rainfalls. These methods include using laser disdrometer (Gires et al. 2020), photographic technique (Pebralia & Amri 2022), methylene paper stain (Zhang et al. 2024) and flour pellet method (Lopes et al. 2025) variants.

The flour pellet method is a practical and cost-effective option where access to advanced equipment is limited. As noted by Sadeghi et al. (2013), the method is well-suited for studies conducted under uncontrolled or resource-constrained environments. It enables the physical capture of drop imprints, which can be measured to determine drop size. One of the method's advantages lies in its independence from electronic systems, reducing susceptibility to calibration errors and power-related failures common in automated instruments. Although the technique requires greater sampling effort and handling, it serves as a

complementary tool, especially for capturing small-diameter raindrops that are often missed by other techniques. While the flour method is less suitable for light rainfall due to the high frequency of very small drops, this is an insignificant limitation for the present study, which focuses on high-intensity rainfall events. Under such conditions, the method performs reliably and avoids many of the operational limitations associated with optical or photographic disdrometers, which can be costly, sensitive to adverse weather, and dependent on frequent recalibration (Sadeghi et al. 2013; Kathiravelu et al. 2016). Furthermore, it circumvents some of the measurement inaccuracies observed with automated disdrometers under heavy rainfall conditions.

A thin, 26 mm layer of wheat flour was used as the target surface for a brief simulated rainfall exposure. To manage the splash-out and pellet overlapping during the calibration phase, three specific control measures were implemented. First, the manual tray exposure was strictly limited to an ultra-brief 1-second window. This restricted time frame maintained a low spatial density of drop impacts across the surface, preventing secondary droplets from falling onto newly formed pellets. Second, a post-exposure pellet count audit was performed to verify that the sample density remained within a non-crowded threshold and any compromised pellet tracks were systematically excluded from the analysis. Finally, because compacted flour beds cause droplets to splash out upon impact, the setup utilized a deep, un-compacted bed of ultra-fine flour. Following exposure, these pellets were then collected, left to dry overnight at a controlled temperature of 105°C, and subsequently subjected to a granulometric analysis. The dried particles were sieved using mesh sizes of 6.30, 5.00, 3.35, 2.36, 2.00, 1.18, and 0.60 mm, and the resulting fractions were weighted, quantified and measured using vernier caliper accordingly by assuming the droplets are sphere in shape.

RAINFALL TERMINAL VELOCITY (V_T) AND ENERGY

Following the measurement of the droplet diameters, the mean raindrops (D_m), V_T, and *KE* of each raindrop were empirically calculated using the established formulae. This approach is due to the inability and practical limitations in direct measurement of *VT* which is essential for direct estimation of rainfall *KE*. For the mean raindrops:

$$D_m = \sqrt[3]{\left(\frac{6}{\pi}\right) W m_R} \quad (2)$$

where D_m is the mean raindrops' diameter (mm) and W is the mean weight of the raindrops (mg) and m_R is the ratio of the mass of the raindrop to the mass of the pellet which is determined using Laws and Parsons (1943) flour-calibration line.

When a raindrop begins to fall, gravity pulls it downward, causing it to accelerate. At the same time, air resistance pushes back against it. As the drop continues falling, these two forces eventually balance out, and the drop reaches a steady speed known as terminal velocity (V_T). This V_T depends largely on the drop's size bigger drops fall faster but also experience more air drag. One common way to estimate this speed is through the Atlas model (Chan et al. 2009) , which uses the formula:

$$V_T = 9.65 - 10.3exp(-0.6D) \quad (3)$$

with D being the diameter (mm). To estimate a drop's volume or mass, it's typically treated as a perfect sphere, using the formula:

$$v = \frac{\pi D^3}{6} \quad (4)$$

From there, the *KE* of the raindrop is calculated using:

$$KE = \frac{1}{2} m v^2 \quad (5)$$

where m is the drop's mass (kg) and v is similar to terminal velocity (m/s). This gives the *KE* of a single droplet. To understand the overall impact of a rain event, researchers add up the *KE* from many droplets to estimate the storm's total *KE*.

RESULTS AND DISCUSSION

RAINFALL SPATIAL UNIFORMITY

The mean CUC for each rainfall intensity was determined based on four replications for each intensity and RS sections, with average recorded values ranging from 81.18% to 88.69% for both RS1 and RS2 respectively as shown in Figure 3. These findings suggest that the rainfall distribution generated by the DRS is considered good, aligns with the standards set by the American Society of Agricultural Engineers (2003). When comparing these results to previous research, particularly studies with test areas similar to this, the findings align closely with reported

CUC. For instance, a paper reported a range of CUC of 82% for a rainfall intensity of 64 mm/hr over a 1.5 m^2 test area (Morin et al. 1967) and 82.1% at 63 mm/hr over 1.2 m^2 test area (Spohr et al. 2015) and 86.2% at 58.6 mm/hr over 1.44 m^2 test area (Pérez-Latorre et al. 2010). While minor improvement in uniformity was observed at higher flow rates, it is worth mentioning that these conditions resulted in extreme rainfall intensities (Lassu et al. 2015).

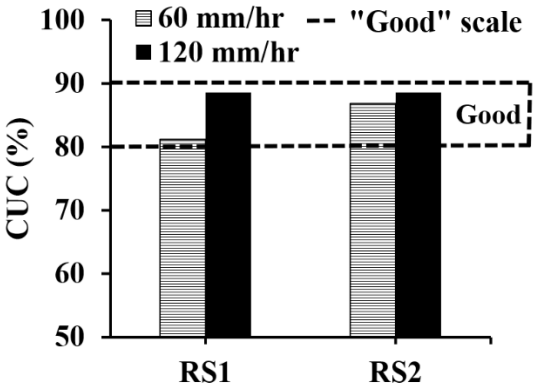


FIGURE 3. CUC percentage for both RS1 and RS2 of different rainfall intensities

RAINFALL DROPLET SIZE DISTRIBUTION

Literature consistently indicates that the droplet size of natural rainfall typically between 0.5 mm to 6 mm in diameter (Ge et al. 2016), with only exceptional cases extending slightly beyond this upper limit (more than 6 mm). In the current study, after careful calibration (accounted for the minor shrinkage observed due to the flour), it was found that the simulated rainfall closely replicated natural raindrop dimensions. Specifically, 90.8% of droplets at a 60 mm/hr intensity, and 92.5% at 120 mm/hr, fell within the 1 mm to 5.9 mm diameter range, a proportion most characteristic of natural precipitation. A comparatively small percentage of raindrops, between 7.5% and 9.2%, were observed to exceed 6 mm in size. This limited occurrence of larger droplets is hypothesized to stem from restricted droplet coalescence, likely attributable to the relatively low fall height within the experimental setup. In addition, the comprehensive analysis of raindrop size distribution in both Figure 4(a) and 4(b) highlighted distinct peaks for the 60 mm/hr intensity, the highest frequency of raindrops (21 droplets) was found in the 2.0–2.4 mm range, while for the 120 mm/hr intensity, the most prevalent size shifted to 5.0–5.4 mm (comprising 32 droplets).

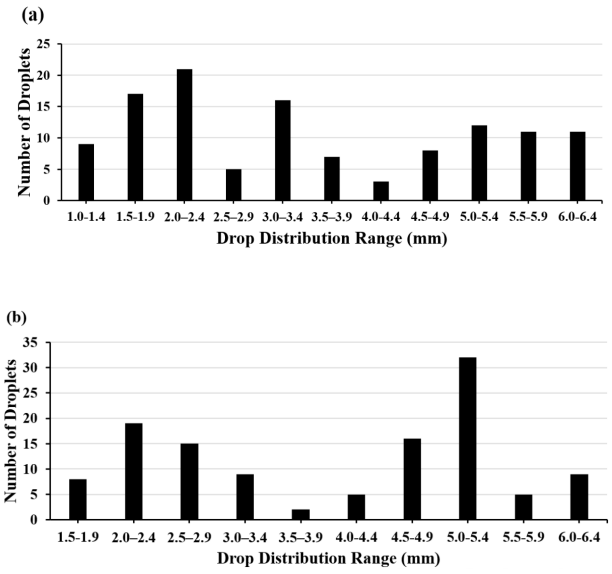


FIGURE 4. Distribution of rainfall droplets across different drop size ranges at (a) 60 mm/hr and (b) 120 mm/hr

Delving into the specifics of DRS, the Raindrop Granulometry (RG) curves in Figure 5 were plotted across various drop diameters and their size-wise percentages passing for each simulation. From these curves, the D_{50} (central values) were extracted for every simulation event, aligning them with the corresponding rainfall intensities. In this current work, the extracted D_{50} values registered at 2.7 mm for the 60 mm/hr intensity and 3.1 mm for the 120 mm/hr intensity, respectively. Although the D_{50} value provides a representative central point in the distribution, it is insufficient to reflect the variability in drop sizes. To better capture this spread, the range between the 25th and 75th percentiles (D_{25}–D_{75}) is also considered. For 60 mm/hr, raindrop diameters ranged from 2 to 4.4 mm, while at 120 mm/hr, they varied from 2.4 to 4.2 mm.

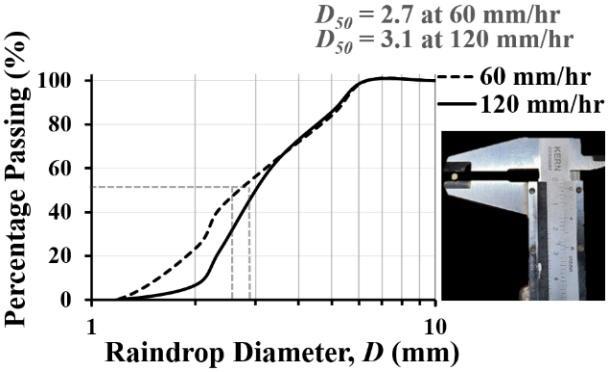


FIGURE 5. RG curve at two different rainfall intensities

Notably, the said D_{50} values, derived from the DRS, fall comfortably within the range documented by Aksoy

(2012) as in Figure 6(b), whose research also proclaim the significant influence of RG on the complex interrelationship between D_{50} and rainfall intensity across various magnitudes. This particular finding supports that as rainfall intensity escalates, there will be concomitant increase in D_{50}. Further quantitative assessment through sieve analysis yielded precise dry pellet weights 3.049 g for the 60 mm/hr rainfall intensity and 4.717 g for 120 mm/hr. Dividing these weights by the respective number of pellets then provided average pellet weights of 25.408 mg and 39.308 mg. Drawing upon the established principles of Laws and Parsons (1943), the mass ratio of raindrop to pellet (m_R) was determined to be approximately 1.12 and 1.14 for the respective intensities. Subsequently, the application of Equation 2 allowed for the precise calculation of the D_m, yielding diameters of 3.8 mm and 4.4 mm for the 60 mm/hr and 120 mm/hr rainfall intensities, respectively as shown in Figure 6(a). Intriguingly, the observed drop size distribution in this study exhibits a negative skewness, where the mean diameter conspicuously exceeds the median. This characteristic pattern powerfully indicates the notable presence of several larger raindrops, which collectively serve to shift the overall average diameter upward within the distribution.

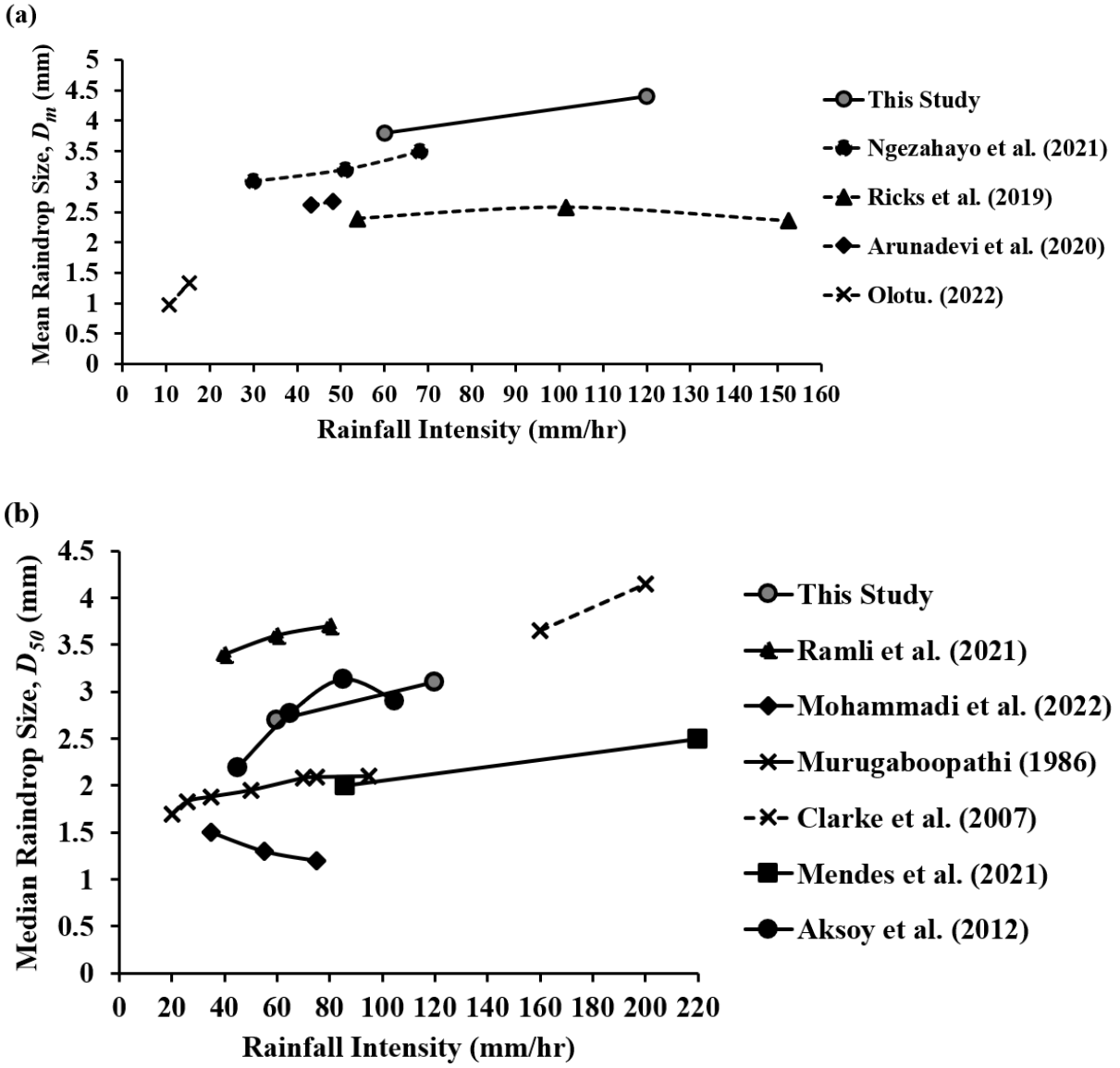


FIGURE 6. Comparison of (a) mean and (b) median raindrop size of simulated raindrops to those reported in prior flour pellet studies

RAINFALL TERMINAL VELOCITY (V_T) AND ENERGY

Based on Table 2 of two simulated intensities of 60 mm/hr and 120 mm/hr, the *KE* per droplet was estimated to be about 1049.61 μJ and 1781.95 μJ each. The increase trend is anticipated as it suits the basic principle of *KE*, which droplet energy will increase together with droplet mass and velocity, as described in Equation 5.

TABLE 2. Derived values of raindrop volume, mass, V_T, and *KE* based on measured rainfall intensities

Rainfall intensity (mm/hr)	Raindrop Volume (mm^3)	Raindrop Mass (mg)	Terminal velocity (m/s)	Kinetic energy (μJ)
60	28.46	28.46	8.59	1049.61
120	44.81	44.81	8.92	1781.95

Meanwhile, Table 3 lists energy flux values obtained from several RS studies. Most of these setups produced droplets larger than 0.4 mm, which explains the higher energy flux in their findings. The analysis, grounded in Equation 5 expressed in terms of the specific energy of the area and depth of the water collected to get the energy flux.

TABLE 3. Energy flux comparison

Mean/Median Raindrop Characteristics			Energy flux ($J/mm/m^2$)	Researcher
Drop size (mm)	Drop velocity (m/s)	Drop height (m)		
0.4 – 2.1	–	12	0.57 – 17.51	(Jadhao et al. 2023b)
2 – 2.5	–	1.58	38.5	(Mendes et al. 2021)
3	–	6.6	18 – 23	(Cottenot et al. 2021)
3.8 – 4.4	8.59 – 8.92	2	36.88 – 39.77	Presented RS
–	–	2	10	(Stašek et al. 2023)

From Table 3, the obtained maximum value of energy flux of the present study is relatively converges to the value reported by Mendes(2021). However, the data distinction from the latter study lies in the fact that an increase in intensity fails to correspond to an increase in energy flux (Cottenot et al. 2021). Their data indicate that the *KE* of the rain is independent of rainfall intensity, attributed to the constant sizes and velocities of the drops as water pressure increases. While extreme setups like the 12 m height (Jadhao et al. 2023b) utilize high fall distances to maximize velocity, they are frequently limited by smaller droplet sizes (0.4–2.1 mm), resulting in a lower overall energy flux (0.57 to 17.51 $J/mm/m^2$). The proposed DRS successfully counterbalances its 2 m structural height constraint by optimizing larger droplet volumes (3.8–4.4 mm), yielding energy flux range of 36.88 to 39.77 $J/mm/m^2$. This output is comparable in magnitude to the energy flux of 38.5 $J/mm/m^2$ reported (Mendes et al. 2021) and the individual peak kinetic-energy values of approximately 38 $J/mm/m^2$ reported in southeastern Australia and northern Nigeria by Van et al. (2002). An individual peak of 41 $J/mm/m^2$ also is documented in New Jersey (Van et al. 2002).

approximately 38 $J/mm/m^2$ reported in southeastern Australia and northern Nigeria by Van et al. (2002). An individual peak of 41 $J/mm/m^2$ also is documented in New Jersey (Van et al. 2002). Consequently, as the produced energy flow coincides with the values documented in the literature, the current simulator is capable of replicating energy flux. Thus, the design is reliable for further use aligning with the expected performance of a DRS despite its compact laboratory footprint.

CONCLUSION

This study presents the design, calibration, and performance evaluation of a DRS tailored for heavy intensities. Calibration of CUC, droplet size distributions, V_T, *KE* and energy flux demonstrated that the system effectively replicates the physical forces of natural precipitation. Notably, while the kinetic energy flux exhibited a linear

dependency on simulated intensity variations, it displayed an inverse relationship with operating pressure due to droplet size optimization at lower pressures. Structural limitations of this configuration must be acknowledged such as the physical 2 m fall height is insufficient for droplets to achieve true natural terminal velocity via gravity alone. Consequently, the V_T and KE calculated represent relative laboratory frameworks rather than absolute open-field equivalents. However, the system's ability to counterbalance this height deficit by optimizing larger droplet volumes (3.8–4.4 mm) yields a mass-driven energy flux that dynamically captures the upper limits of natural global storm profiles. This confirms that high spatial uniformity and realistic energy replication can be achieved on a plot scale without requiring an excessively tall structure. These findings can be directly applied in subsequent experimental plots to evaluate soil splash erosion dynamics and slope stability modeling. Specifically, future work can focus on integrating automated pressure-regulating pumps with variable dripper nozzle sizes to gain control over the droplet size.

ACKNOWLEDGEMENT

We would like to thank the Universiti Sains Malaysia for partially supporting the postgraduate student through Short Term Grant of STG#2024/206/ST5505 under account R501-LR-RND002-0000000334-0000.

DECLARATION OF COMPETING INTEREST

None.

REFERENCES

Aksoy, H., Unal, N.E., Cokgor, S., Gedikli, A., Yoon, J., Koca, K., Inci, S.B. & Eris, E. 2012. A rainfall simulator for laboratory-scale assessment of rainfall-runoff-sediment transport processes over a two-dimensional flume. *Catena* 98: 63–72.

Anderson, R.L., Rowntree, K.M. & Le Roux, J.J. 2021. An interrogation of research on the influence of rainfall on gully erosion. *Catena* 206: 105482.

Costa, A.R.D.S., Alvarenga, L.A., Thebaldi, M.S., Lima, L.A., Colombo, A., Green, D. & Isidoro, J.M.G.P. 2024. Characterization of artificial rainfall produced by a portable rainfall simulator using a rotating dynamic rainfall gauge system. *Hydrological Sciences Journal* 69(9): 1218–1227. https://doi.org/10.1080/02626667.2024.2368266

American Society of Agricultural Engineers. 2003. *ASAE EP405.1: Design and Installation of Microirrigation Systems*. St. Joseph, MI: American Society of Agricultural Engineers.

Bosio, R., Cagninei, A. & Poggi, D. 2023. Large laboratory simulator of natural rainfall: From drizzle to storms. *Water* 15(12): 2205.

Boulange, J., Malhat, F., Jaikaew, P., Nanko, K. & Watanabe, H. 2019. Portable rainfall simulator for plot-scale investigation of rainfall-runoff, and transport of sediment and pollutants. *International Journal of Sediment Research* 34(1): 38–47.

Chan, E.-S., Lee, B.-B., Ravindra, P. & Poncelet, D. 2009. Prediction models for shape and size of Ca-alginate macrobeads produced through extrusion–dripping method. *Journal of Colloid and Interface Science* 338(1): 63–72.

Christiansen, J.E. 1942. *Irrigation by Sprinkling*. Bulletin 670. Berkeley, CA: California Agricultural Experiment Station, University of California.

Costa, A.R.D.S., Alvarenga, L.A., Thebaldi, M.S., Melo, P.A., Colombo, A. & Isidoro, J.M.G.P. 2023. Portable rainfall simulator: Evaluation and suitability of plot geometry to improve rainfall uniformity. *Engenharia Sanitária e Ambiental* 28: e20220198. https://doi.org/10.1590/S1413-415220220198

Cottenot, L., Courtemanche, P., Nouhou-Bako, A. & Darboux, F. 2021. A rainfall simulator using porous pipes as drop former. *Catena* 200: 105101.

D'Angelo, O., Kuthe, F., Van Nieuwland, K., Ederveen Janssen, C., Voigtmann, T. & Jalaal, M. 2022. Spreading of droplets under various gravitational accelerations. *Review of Scientific Instruments* 93(11): 115103.

Ehsan, S., Yasir, Q.M., Awais, R.M., Sattar, T., Mustafa, G. & Fida, U. 2024. Modelling of riverine flooding using HEC-RAS—A case study of Badri Khawar River in KPK, Pakistan. *Jurnal Kejuruteraan* 36(1): 169–177. https://doi.org/10.17576/jkukm-2024-36(1)-16

Felipe, A.J.B., Baguio, M.A. & Saludes, R.B. 2024. Modeling assessment on the influences of physiographic dynamics of landscape and micro-climatic conditions at Siffu-Mallig watershed in the Philippines. *Modeling Earth Systems and Environment* 10(4): 5329–5350.

Fernández, R.M., Rodríguez, I., Caldevilla, P., Búrdalo, G., Ortiz, A. & Martínez-García, R. 2022. Optimization of a laboratory rainfall simulator to be representative of natural rainfall. *Water* 14(23): 3831.

Gabyshev, D.N., Szakáll, M., Shcherbakov, D.V., Fedorets, A.A. & Dyachkov, S.M. 2022. Oscillatory signatures in the raindrop motion relative to the air medium with terminal velocity. *Atmosphere* 13(7): 1137.

Ge, M., Wu, P., Zhu, D. & Ames, D.P. 2016. Comparison between sprinkler irrigation and natural rainfall based on droplet diameter. *Spanish Journal of Agricultural Research* 14(1): e1201.

Gires, A., Bruley, P., Ruas, A., Schertzer, D. & Tchiguirinskaia, I. 2020. Disdrometer measurements under Sense-City rainfall simulator. *Earth System Science Data* 12(2): 835–845.

Green, D. & Pattison, I. 2022. Christiansen uniformity revisited: Re-thinking uniformity assessment in rainfall simulator studies. *Catena* 217: 106424. https://doi.org/10.1016/j.catena.2022.106424

Hamizak, S.N., Suif, Z., Jelani, J. & Ahmad, N. 2024. Dynamic of sediment transport capacity by overland flow: A review. *Jurnal Kejuruteraan* 36(5): 2019–2034.

Idrus, J., Ramli, R., Md Nujid, M. & Sadikon, S.F. 2023. Enhancing slope stability with different slope stabilization measures: A case study using SLOPE/W software. *Jurnal Kejuruteraan* 35(6): 1427–1434.

Jadhao, V.G., Pandey, A. & Mishra, S.K. 2023a. Modeling of rain erosivity employing simulated rainfall and laser precipitation monitor. *Modeling Earth Systems and Environment* 9(4): 4477–4492. https://doi.org/10.1007/s40808-023-01727-0

Jadhao, V.G., Pandey, A. & Mishra, S.K. 2023b. Sediment modeling using laboratory-scale rainfall simulator and laser precipitation monitor. *Environmental Research* 237: 116859. https://doi.org/10.1016/j.envres.2023.116859

Jwa, M., Jin, H.-G., Lee, J., Moon, S. & Baik, J.-J. 2021. Characteristics of raindrop size distribution in Seoul, South Korea according to rain and weather types. *Asia-Pacific Journal of Atmospheric Sciences* 57(3): 605–617.

Kalehhouei, M., Sadeghi, S.H., Khaledi Darvishan, A. & Hasanzadeh, N. 2025. In-depth dynamic analysis of raindrop characteristics under varying intensities using image processing. *Hydrological Sciences Journal*. https://doi.org/10.1080/02626667.2025.2508892

Kathiravelu, G., Lucke, T. & Nichols, P. 2016. Rain drop measurement techniques: A review. *Water* 8(1): 29.

Kinnell, P.I.A. 2022. Insights into the sediment transport processes operating in rain-impacted flows. *Catena* 217: 106452.

Lanza, L.G., Merlone, A., Cauteruccio, A., Chinchella, E., Stagnaro, M., Dobre, M., Garcia Izquierdo, M.C., Nielsen, J., Kjeldsen, H., Roulet, Y.A., Coppa, G., Musacchio, C., Bordianu, C. & Parrondo, M. 2021. Calibration of non-catching precipitation measurement instruments: A review. *Meteorological Applications* 28(3): e2002.

Lassu, T., Seeger, M., Peters, P. & Keesstra, S.D. 2015. The Wageningen rainfall simulator: Set-up and calibration of an indoor nozzle-type rainfall simulator for soil erosion studies. *Land Degradation & Development* 26(6): 604–612.

Laws, J.O. & Parsons, D.A. 1943. The relation of raindrop-size to intensity. *Eos, Transactions American Geophysical Union* 24(2): 452–460.

Lazarus, R.R., Wan Jaafar, W.Z., Alengaram, U.J. & Hin, L.S. 2023. Overview of the research gaps in the rainfall simulator study. *Soil Science Society of America Journal* 87(6): 1231–1248.

Li, T., Liang, C., He, B. & Li, S. 2023. Effects of cornstalk mulching and rainfall intensity on the quantity and quality of dissolved organic carbon in runoff: A field rainfall simulation at the plot scale. *Land Degradation & Development* 34(13): 3920–3931.

Li, X., Cai, X., Li, S., Huang, X., Zhu, C. & Xu, H. 2025. Analysis of the structural behavior evolution of reinforced soil retaining walls under the combined effects of rainfall and earthquake. *Buildings* 15(1): 115. https://doi.org/10.3390/buildings15010115

Lopes, I., De Lima, J.L.M.P., Montenegro, A.A.A. & Carvalho, A.A.D. 2025. Assessment of water retention and absorption of organic mulch under simulated rainfall for soil and water conservation. *Soil Systems* 9(1): 4.

Maroufpoor, E., Faryabi, A., Ghamarnia, H. & Moshrefi, G.Y. 2010. Evaluation of uniformity coefficients for sprinkler irrigation systems under different field conditions in Kurdistan Province (northwest of Iran). *Soil and Water Research* 5(4): 139–145.

Mendes, T.A., Alves, R.D., Gitirana, G.D.F.N., Pereira, S.A.D.S., Rebolledo, J.F.R. & Da Luz, M.P. 2021. Evaluation of rainfall interception by vegetation using a rainfall simulator. *Sustainability* 13(9): 5082.

Morin, J., Goldberg, D. & Seginer, I. 1967. A rainfall simulator with a rotating disk. *Transactions of the ASAE* 10(1): 74–77. https://doi.org/10.13031/2013.39599

Nguyen, P.T., Vo, L.N., Dang, T.X., Tran, H.V.V. & Nguyen, T.A. 2025. Assessment of the impact of pile characteristics on the horizontal displacement of retaining walls under heavy rainfall: A case study in Vietnam. *Engineering, Technology & Applied Science Research* 15(2): 21208–21213.

Pebralia, J. & Amri, I. 2022. A low-cost and practical method for determining raindrop size from spray nozzle by using a mobile phone camera. In *Proceedings of the International Conference on Radioscience, Equatorial Atmospheric Science and Environment and Humanosphere Science, 2021*, 449–455. Singapore: Springer Nature.

Pérez-Latorre, F.J., De Castro, L. & Delgado, A. 2010. A comparison of two variable intensity rainfall simulators for runoff studies. *Soil and Tillage Research* 107(1): 11–16.

Pietro, M.S.M., Ferreira Pinto, M., Alves Sobrinho, T., Schultz, N., Altamir Rodrigues Coutinho, T. & Fonseca De Carvalho, D. 2021. A modified portable rainfall simulator for soil erosion assessment under different rainfall patterns. *Journal of Hydrology* 596: 126052.

Rajamoorthy, Y. & Munusamy, S. 2018. Evidence of electricity consumption lead climate change in Malaysia. *Jurnal Kejuruteraan* SI 1(6): 49–58.

Ramli, H., Mohd Yusoff, S.A.N., Azmi, M., Sabtu, N. & Hezmi, M.A. 2021. Influence of drop size distribution and kinetic energy in precipitation modelling for laboratory rainfall simulators. *Hydrology and Earth System Sciences Discussions*: 1–23. https://doi.org/10.5194/hess-2021-462

Ren, F., Huang, Q. & Chen, J. 2022. Centrifuge modeling of geosynthetic-reinforced soil retaining walls subjected to the combined effect of earthquakes and rainfall. *Geotextiles and Geomembranes* 50(3): 470–479.

Ren, Z., Zhang, X., Zhang, X., Li, Z., Li, P. & Zhou, Z. 2021. Sand cover enhances rill formation under laboratory rainfall simulation. *Catena* 205: 105472.

Renner, C., Conroy, N., Thaler, E., Collins, A., Thomas, L., Dillard, S., Rowland, J. & Bennett, K. 2024. The Next-Generation Ecosystem Experiment Arctic rainfall simulator: A tool to understand the effects of changing rainfall patterns in the Arctic. *Hydrology Research* 55(1): 67–82.

Rončević, V., Živanović, N., Ristić, R., Van Boxel, J.H. & Kašanin-Grubin, M. 2022. Dripping rainfall simulators for soil research—Design review. *Water* 14(20): 3309.

Sadeghi, S.H., Abdollahi, Z. & Darvishan, A.K. 2013. Experimental comparison of some techniques for estimating natural raindrop size distribution on the south coast of the Caspian Sea, Iran. *Hydrological Sciences Journal* 58(6): 1374–1382.

Spohr, R., Corcini, A., Pellegrin, J., Bonfanti, J., Soto, M. & Cardoso, T. 2015. Desenvolvimento e validação de um simulador de chuvas portátil. *Revista Brasileira de Recursos Hídricos* 20(2): 411–417.

Stašek, J., Krása, J., Mistr, M., Dostál, T., Devátý, J., Středa, T. & Mikulka, J. 2023. Using a rainfall simulator to define the effect of soil conservation techniques on soil loss and water retention. *Land* 12(2): 431.

Suif, Z., Ahmad, N., Jelani, J., Isa, N.A. & Farhani, N.N. 2025. Spatio-temporal patterns of soil erosion and sediment yield in the UPNM catchment. *Jurnal Kejuruteraan* 37(3): 1505–1514.

Tiller, M., Reading, L., Miska, M. & Egodawatta, P. 2025. Analysis of square pattern spray nozzles for use in a portable field rainfall simulator. *Catena* 250: 108796.

Van Dijk, A.I.J.M., Bruijnzeel, L.A. & Rosewell, C.J. 2002. Rainfall intensity-kinetic energy relationships: A critical literature appraisal. *Journal of Hydrology* 261: 1–23.

Xiao, H., Xiang, R., Yan, R., Xia, Z., Guo, P., Gao, F., Zhang, W., Zhu, Z., Dong, X., Zhang, L., Yang, Y. & Kang, C. 2024. Evaluating the influences hedgerow on soil erosion and nitrogen loss of purple soil sloping farmland under simulated rainfall. *Ecological Indicators* 158: 111438.

Yang, T., Niu, J., Fan, D., Wang, D., Miao, Y., Wang, M., Zhao, C., Zhang, L., Chen, X. & Berndtsson, R. 2025. Wind and rainfall erosion energy in large sediment generating and coarse sediment class areas of the Middle Yellow River. *International Soil and Water Conservation Research* 13(1): 67–79.

Yonter, G. & Houndonougbo, H.M. 2022. Comparison of different fulljet nozzles used in laboratory type rain simulator in terms of some rainfall characteristics. *Ege Üniversitesi Ziraat Fakültesi Dergisi* 59(1): 33–41.

Zhang, R., Liu, Y., Zhu, D., Wu, P., Xia, W., Zheng, C. & Zhang, X. 2024. Comparative analysis of micro-physical characteristics of sprayed droplets using various measurement technologies. *Irrigation Science* 42(4): 701–719.

Zhang, S.-Y., Zhuo, M., Xie, Z., Yuan, Z., Wang, Y., Huang, B., Liao, Y., Li, D. & Wang, Y. 2020. Effects of near soil surface components on soil erosion on steep granite red soil colluvial deposits. *Geoderma* 365: 114203.

Živanović, N., Rončević, V., Spasić, M., Ćorluka, S. & Polovina, S. 2022. Construction and calibration of a portable rain simulator designed for the in situ research of soil resistance to erosion. *Soil and Water Research* 17(3): 158–169.